Proceedings of the ASME 2019
International Design Engineering Technical Conferences
and Computers and Information in Engineering Conference
IDETC/CIE2019
August 18-21, 2019, Anaheim, CA, USA

# IDETC2019-97888

# ACOUSTIC NON-RECIPROCAL BAND STRUCTURE IN A PASSIVE, NONLINEAR, 1D MATERIAL

# Lezheng Fang

Graduate Student
George W. Woodruff School of Mechanical
Engineering, Georgia Institute of Technology
Atlanta, GA 30332, USA
lezheng.fang@gatech.edu

#### Alexander F. Vakakis

Professor
Department of Mechanical Science and
Engineering, University of Illinois at UrbanaChampaign
Champaign, IL 61820, USA
avakakis@illinois.edu

#### **ABSTRACT**

Acoustic non-reciprocity, referring to the phenomenon of path-dependent propagation, has diverse applications in mechanical devices. This paper presents a numerical study on a periodic triangle-shape structure that breaks reciprocity in a passive manner over a broad range of frequency and energy. The proposed structure contains strong nonlinearity and geometric asymmetry, which contributes to a direction-dependent dispersion relationship. When the signal frequency falls in the band pass in one direction, and band gap in the other, a unidirectional wave propagation results. The system achieves giant non-reciprocity with minimal distortion in the frequency content of the signal.

**Keywords**: 1-D periodic structure, strongly nonlinear, asymmetric, non-reciprocity, dispersion relationship analysis.

### **Amir Darabi**

Postdoctoral Fellow
George W. Woodruff School of Mechanical
Engineering, Georgia Institute of Technology,
Atlanta, GA 30332, USA; Department of
Mechanical Science and Engineering, University
of Illinois at Urbana- Champaign, Champaign, IL
61820, USA
amirdarabi@gatech.edu

# Michael J. Leamy\*

Professor School of Mechanical Engineering Georgia Institute of Technology Atlanta, GA 30332, USA michael.leamy@me.gatech.edu

#### INTRODUCTION

In linear time-invariant system, wave transmission between two points in space is independent of the propagation direction [1, 2]. Such symmetry, called acoustic reciprocity, is widely observed, and related to the Onsager-Casimir principle [3, 4]. Non-reciprocity violates this property and shows the possibility of controlling wave propagation and engineering desired propagation patterns (e.g., allowing the propagation in one direction but not the other way around [5]).

To break reciprocity, multiple approaches have been studied. The common method is to apply an external asymmetry bias to the system, such as adding an odd-symmetry magnetic field or fluid circulation into the system [6]. Another approach achieves non-reciprocity through utilizing time-variant parameters, for instance, periodically modulating the density and modulus in space and time [7, 8]. However, the aforementioned attempts are restricted by the necessity of either external bias or additional control.

<sup>\*</sup>Address all correspondence to this author.

Breaking reciprocity via passive manners, on the other hand, does not rely on the external asymmetry bias. One possible technique is to combine structural asymmetry and nonlinearity together to achieve non-reciprocity. Such systems utilize the band diagram of the structure to filter the wave based on the frequency. Liang et al [9, 10], numerically and experimentally, developed an acoustic rectifier by attaching the nonlinear materials to a super-lattice, where the signal frequency falls in the band gap while the second harmonic generated by nonlinear material falls in the band pass. Later, the authors in [11, 12] theoretically and experimentally demonstrated the feasibility of an acoustic diode based on nonlinear coupling and asymmetrical hierarchy internal structure. Recently, Li proposed a theoretical wave diode utilizing asymmetric shapes of nonlinear materials. and analyzed its non-reciprocal behavior by solving the discrete nonlinear Schrödinger equation [13]. To achieve non-reciprocity, most of the passive systems reviewed above either changes the frequency content of the sending signal, or has a strict restriction on the range of sending frequency.

Inspired by the structure in [13], in this paper, we propose and numerically study a nonlinear, asymmetric and periodic system, which passively breaks reciprocity for a range of input frequency and amplitude, with minimal distortion of the sending frequency. The physical mechanism behind the non-reciprocity is a direction-dependent dispersion relationship of the periodic structure due to its triangle-shaped asymmetry and strongly nonlinear couplings. Thus, the range of input frequency causing non-reciprocity is related to the band structure of the system and can be tuned by varying the input amplitude. Additionally, when the sending frequency falls in the passband of the system, the frequency content is in general well-preserved.

#### SYSTEM DESCRIPTION

The proposed system consists of a chain of unit cells, each composed of a finite number of masses coupled by linear and nonlinear springs and dampers. Figure 1(a) depicts an isolated unit cell from the chain. Each of the unit cells contains 16 identical masses. As shown in the Figure 1(b), the green coupling represents a linear spring paralleled with a linear viscous damper; the red coupling contains a linear spring, a linear viscous damper and a cubic stiffness spring. Note that the two linear springs  $(k_1 \text{ and } k_2)$  have different stiffness.

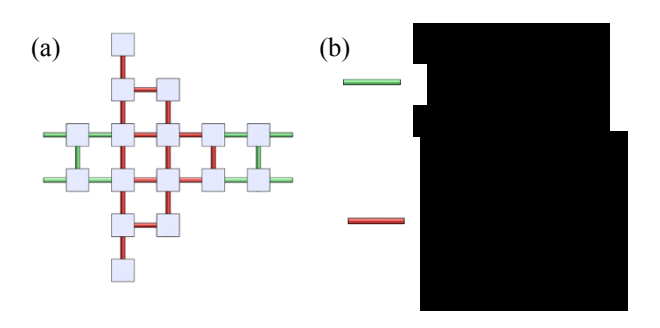


Figure 1. A schematic of (a) an isolated unit cell and (b) the spring-damper model for the coupling

The system represents a shear lattice in which every mass moves only in a direction perpendicular to the lattice plane. Equation of motion concerning a mass in the periodic structure is provided below

$$m\ddot{x}^* + c\Sigma(\dot{x}^* - \dot{x}_p) + k_1\Sigma(x^* - x_i) + k_2\Sigma(x^* - x_j) + k_{NL}\Sigma(x^* - x_j)^3 = 0.$$
(1)

Here,  $x^*$  denotes the displacement of the studied mass; the subscription p denotes the adjacent mass connected with the studied mass, and subscriptions i and j refer to the adjacent mass connected with the studied mass by green and red coupling respectively. The system parameters are provided below.

Table 1. System parameter values for the triangle-shape unit cell

| Parameter | Value             | Unit    |
|-----------|-------------------|---------|
| m         | 0.05              | kg      |
| c         | 0                 | kg/s    |
| $k_1$     | 200               | N/m     |
| $k_2$     | 20                | N/m     |
| $k_{NL}$  | 2x10 <sup>9</sup> | $N/m^3$ |

To study the dispersion relationship of the periodic structure, we build a finite system in numerical simulation. The finite system contains three parts: i) a linear waveguide, ii) 40 proposed unit cells, and iii) non-reflective boundary at the end. The waveguide is a two-layer monatomic chain connected via green coupling as shown in Figure 2. Note that the waveguide is undamped and sufficiently long so that after the signal hits the triangle-shaped unit cells, the reflected waves do not interfere with the source, which guarantees the equality of input energy for both directions. The non-reflective boundary domain contains 10 triangle-shaped unit cells with the damping increasing exponentially along the chain. At the end of the chain, the amplitude of signal is ensured to be sufficiently small. Such design avoids the reflection at the tail of the chain and therefore makes it possible to use a finite system to study a periodic structure.

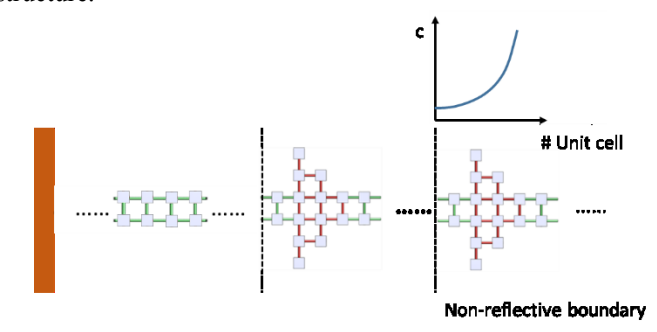


Figure 2. Schematic of the infinite chain model.

The input signal is generated by a continuous harmonic oscillation in force control and applied to the system at the beginning of the waveguide. Note that the boundary mass where force is applied is grounded by a linear spring with the stiffness of  $k_1$ . Hann window function is utilized here to control the amplitude of the signal for a smoother wave introduction, shown as below

$$A^* = hA \tag{2}$$

$$h = 0.5 - 0.5\cos\left(\frac{t\pi}{nT}\right) \quad t \in [0, nT],\tag{3}$$

where  $A^*$  is the input amplitude tuned by the Hann window factor  $\mathbf{h}$ . In Equation (3), the Hann window factor  $\mathbf{h}$  is a function of time  $\mathbf{t}$ , cycles of sending signal  $\mathbf{n}$ , and input period  $\mathbf{T}$ . As shown in Figure 3, after  $\mathbf{n}$  cycles, the signal develops to its full amplitude.

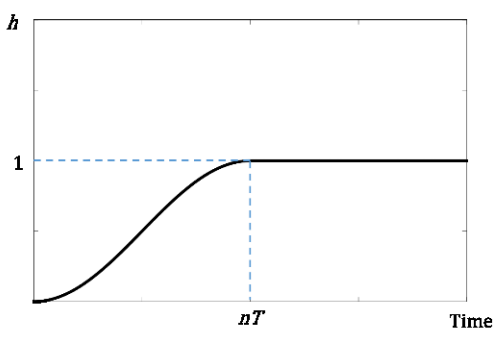


Figure 3. The growth of Hann window factor as a function of time.

The equation of motion concerning the starting mass with excitation is provided below.

$$m\ddot{x} + k_1 \Sigma (x - x_i) + k_1(-x) + c\Sigma (\dot{x} - \dot{x}_p) = hAcos(\omega t)$$
(4)

# **ANALYSIS APPROACH**

This section discusses i) an analytical approach to find the dispersion relationship of two linear cases of the system, and more importantly, ii) the numerical approach to find the amplitude-dependent dispersion relationship. It should be mentioned that the main focus of the dispersion analysis in this study is on the acoustic branch. The optical branches are ensured to be sufficiently far from frequency range of interest.

Analytically, the dispersion relationship of a periodic linear structure can be obtained by solving the eigenvalue problem from the Bloch theorem shown below, where  $\mu$  denotes wavenumber,  $\omega$  denotes frequency, and M and K denote mass matrix and stiffness matrix respectively [15].

$$[\kappa(\mu) - \omega^2 \mathbf{M}] \tilde{\mathbf{u}}(\mu) e^{in\mu} = 0 \tag{5}$$

$$\boldsymbol{\kappa}(\mu) = \boldsymbol{\Sigma}_{m=-1,0,+1} \left( e^{im\mu} K_m \right) \tag{6}$$

For systems containing nonlinear components, such as the cubic springs in the proposed structure, Bloch theorem can predict the dispersion relationship only for certain conditions. Since the stiffness of the cubic spring depends upon the input energy, when the input energy is very low, the response from the nonlinear spring is negligible compared to the linear coupling. On the opposite, when the input energy is very high, the nonlinear spring has a much higher stiffness than the linear coupling, and can be treated as rigid connection. In both conditions, the system shows a strong linear pattern, where Block theorem can be applied.

To better understand the amplitude-dependent dispersion relationship, we numerically model the system in MATLAB, and use ode45 as our main solver for differential equations. Responses of broadband (frequency and amplitude) excitation are studied. For each signal, we measure the wavenumber of the response in the nonlinear unit cells using a relative wavenumber method. Specifically, the first masses of two adjacent nonlinear unit cells near the signal source are selected. The Fast Fourier Transformation (FFT) is then applied in the steady state of the time response measured at the selected masses. The FFT result gives the dominant frequency for each mass and its corresponding amplitude and phase. Then the difference of the phase reveals the real part of the local wavenumber. Equations governing the wavenumber calculation are shown here [16],

$$a(\omega) = Re(G(\omega)) \tag{7a}$$

$$b(\omega) = Im(G(\omega)) \tag{7a}$$

$$\theta(\omega) = \tan^{-1}(\frac{b(\omega)}{a(\omega)}) \tag{8}$$

$$Re(\mu) = \theta_n(\omega^*) - \theta_{n+1}(\omega^*), \tag{9}$$

where  $G(\omega)$  is the magnitude of frequency  $\omega$ , and  $\omega^*$  denotes the dominant frequency. Finally, the resultant wavenumber is then re-scaled to be between  $-\pi$  and  $\pi$ . Note that the spatial FFT method is not preferred here because there are only 40 unit cells (sample points) in the structure, which restricts the resolution of spatial FFT.

#### **RESULTS**

This section presents the analytical solution of the dispersion relationship of two linear cases and the numerical results concerning i) asymmetric dispersion surface/curve, ii) non-reciprocal propagation represented in time responses, and iii) the non-reciprocal energy transmission in an optimized model.

By solving the eigenvalue problem from Equation (5), the dispersion relationship of two linear cases are obtained and displayed in Figure. 4. It shows the dispersion relationship of the system in two linear cases: i) high energy input and ii) low

energy input. These two curves define the boundaries of our system, from purely linear (low energy) to rigid-linear (high energy).

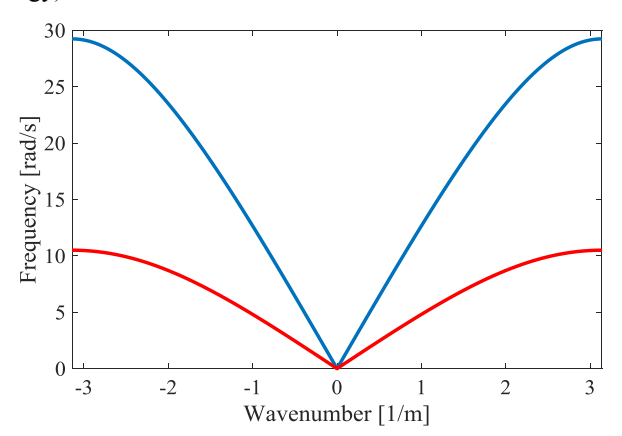


Figure 4. Analytical result of dispersion relationships (only acoustic branch) in high (red curves) /low (blue curves) energy regimes. Positive wavenumber stands for left-to-right propagation and negative wavenumber being right-to-left propagation.

Numerically, the steady-state wavenumber of a mass depends upon the sending signal frequency and amplitude. One signal frequency and one amplitude only yield one steady-state wavenumber for a given mass. Therefore, when varying the sending frequency signal and amplitude, we can obtain a cloud of scatter points in 3D, with 3 axes being wavenumber, frequency, and amplitude. Most obtained scatter points fit a sinusoidal trend. However, considerable numerical errors happen for the points near the edge of the First Brillion Zone (FBZ), where their wavenumbers approach  $\pm \pi$ . These data points are revised by curve fits in both the frequency-wavenumber plane and frequency-displacement plane. Eventually, the dispersion surface shown in Figure 5(a) is obtained from a fine surface meshing.

In Figure 5(b), we select the dispersion curves highlighted in Figure 5(a), and depict both left-to-right (L-R) propagation and right-to-left (R-L) propagation in the positive wavenumber domain. L-R propagation is represented in solid line and R-L is represented by dashed lines. Here, we can see clearly that as the input amplitude increases, both dispersion curves rises, yet to different height, and the gap between the L-R and R-L dispersion curve can be tuned by varying sending amplitude. In Figure 5(c), we select the purple color dispersion curve in Figure (b) and present it in the wavenumber-frequency plane. Note that the red and blue dispersion curves depict the low energy and high energy extreme respectively. Non-reciprocity is observed - the L-R propagation has a higher dispersion curve than the R-L propagation, and a strong non-reciprocity region is generated-in between the two dashed lines. Any frequency that falls in this region is in the band pass for L-R, but band gap for R-L, thus can only propagate to the right.

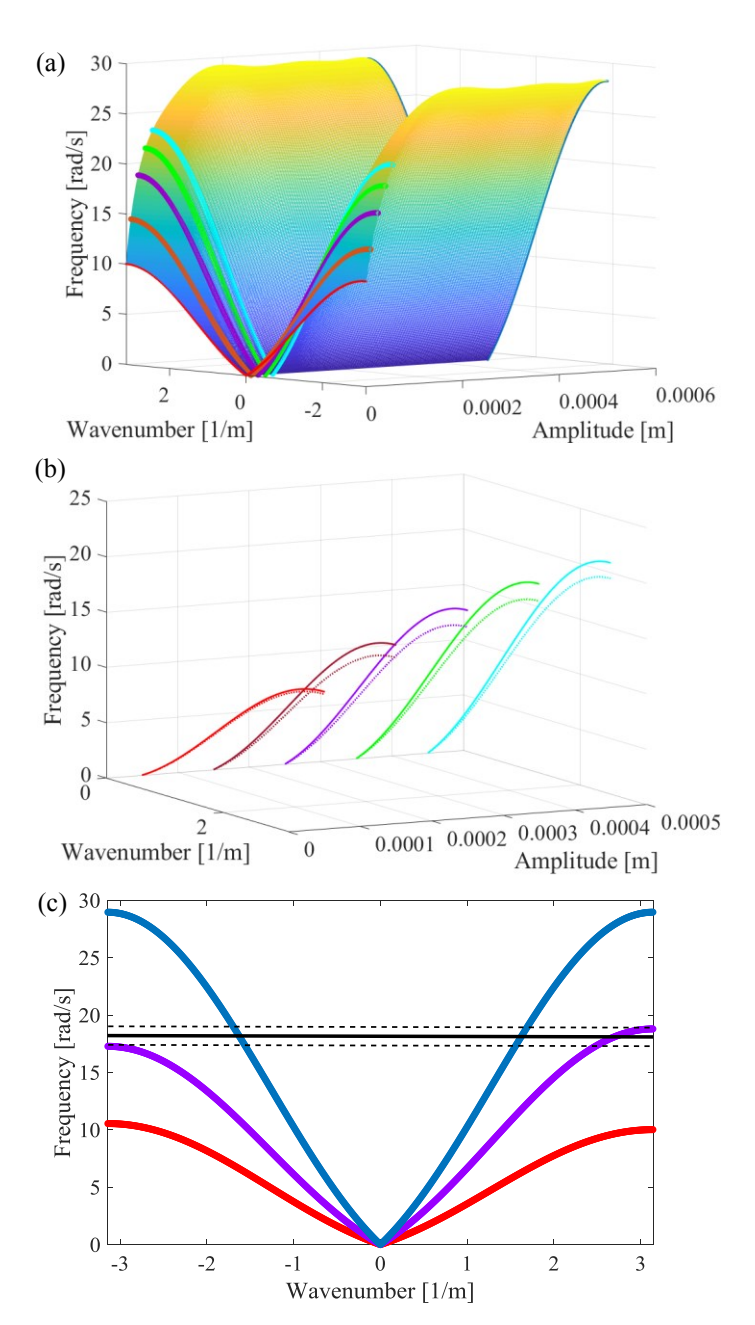


Figure 5. (a) The dispersion surface numerically obtained. Selected dispersion curves are highlighted. (b) Selected slices from the dispersion surface, with solid lines represent L-R propagation, and dashed lines represent R-L propagation. (c) A detailed view of the purple dispersion curve, with the red and blue curves represent the low-energy extreme and high-energy extreme respectively. Note that the range of frequency causing non-reciprocity is enclosed by two dashed line. An example frequency (black solid line) is picked, and response of which is shown in later work.

To verify such non-reciprocity in time response, we send a signal with the sending frequency and amplitude in the non-reciprocity zone, shown as the solid line in Figure 5(c). The displacement and frequency responses of the same mass are plotted in Figure 6(a) and 6(b).

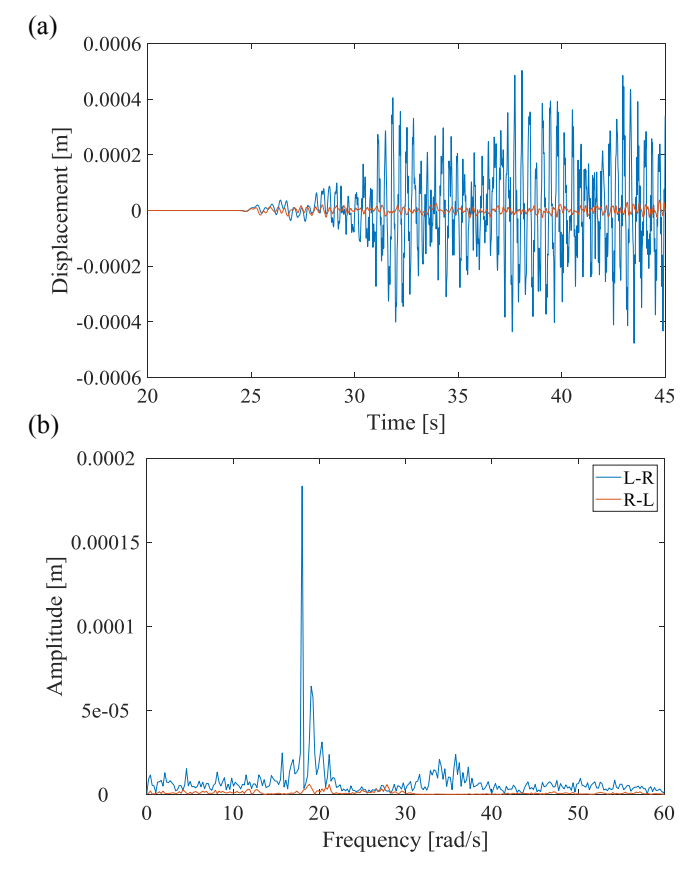


Figure 6. The time and frequency response of the input signal shown in Fig. 5(c).

Clearly, the wave propagates in the L-R direction, while only minor noise comes through the other way. The propagating L-R wave now has a richer frequency content because of the nonlinear components; however, the induced frequencies do not change the dominance of the sending frequency.

As the non-reciprocity in time response is observed, the energy transmission of the proposed structure is of interest to study. To investigate the energy transmission, we replace the non-reflective boundary domain by another linear waveguide and grounding its end. Now, the triangle-shape unit cells are sandwiched by two identical waveguides where signals can be sent and received. The schematic is shown in Figure 7.

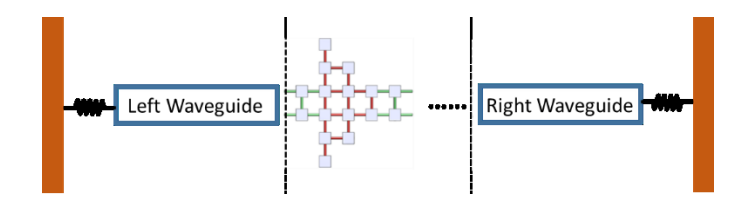


Figure 7. Schematic of the model used to study energy transmission.

Three other changes are added to the model: i) the number of the triangle-shaped unit cells is reduced to three, ii) the damping is removed from this system, and iii) the masses and springs in the unit cells are preliminarily optimized. The first change is to avoid the situation that the signal disperses too much energy in the long nonlinear unit cells. In this scenario, very little energy reaches the receiving waveguide, which makes the transmission ratio always low. The second change simplifies the problem by maintaining the total energy in the system the same. Finally, the third change aims to increase the asymmetry of a unit cell by changing the mass and spring stiffness at certain locations. See Figure 8 and Table 2 for more details.

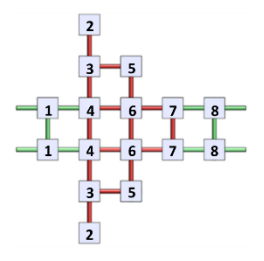


Figure 8. Schematic graph of the unit cell after preliminarily optimization.

Table 2. Optimized mass and spring stiffness values

| Parameter | Value  | Unit |
|-----------|--------|------|
| $m_1$     | 0.05   | kg   |
| $m_2$     | 0.0616 | kg   |
| $m_3$     | 0.0733 | kg   |
| $m_4$     | 0.07   | kg   |
| $m_5$     | 0.05   | kg   |
| $m_6$     | 0.05   | kg   |
| $m_7$     | 0.3911 | kg   |
| $m_8$     | 0.05   | kg   |
| $k_{1-4}$ | 400    | N/m  |

Here,  $m_1 - m_8$  represents the masses shown in Figure 8, and  $k_{1-4}$  stands for the linear spring stiffness between  $m_1$  and  $m_4$ . The stiffness of other springs in green connections remains unchanged, with the normalized value of 1. Note that, a

chain composed by such unit cells has an "up-down" symmetry, and the wave propagation is only one dimensional.

A different excitation method is employed in this model to i) send finite cycles of plane wave instead of continuous signal, ii) reduce the time complexity of the simulation [14]. The excitation is realized by modifying the initial conditions (displacement and velocity) of masses at the boundary of the waveguide and the nonlinear unit cells domain to prepare a steady-state plane wave that propagates towards the nonlinear unit cells. The equations that represent such initial conditions are provided below:

$$\mu(\omega) = \cos(1 - \frac{m\omega^2}{2k_1}) \tag{10}$$

$$y|_{L-R}(t,x_i)|_{t=0} = A\cos(-\mu(x_L^* - x_i))$$
 (11a)

$$\dot{y}|_{L-R}(t,x_i)|_{t=0} = A\omega \sin(-\mu(x_L^* - x_i))$$
 (11b)

$$y|_{R-L}(t,x_j)|_{t=0} = A\cos(-\mu(x_j - x_R^*))$$
 (12a)

$$\dot{y}|_{R-L}(t,x_j)|_{t=0} = -A\omega\sin\left(-\mu(x_j - x_R^*)\right) \quad (12b)$$

As shown in equation (10), the wavenumber of the sending signal can be obtained from the dispersion relationship in linear waveguide. Equation (11) and (12) depict the initial conditions for L-R and R-L propagation respectively, where  $x_L^*$  and  $x_R^*$  denote the location of the left and right boundary of the triangle-shaped unit cells domain respectively;  $x_i$  and  $x_j$  refer to the location of the mass where we change its initial conditions. Note that the signal is excited at the left waveguide with a right-towards wavenumber for L-R propagation, and excited at the right waveguide with a left-towards wavenumber for R-L propagation. For both L-R and R-L cases, the signal has the same length, and thus the same energy.

To study the energy transmission pattern in the second model, the system is first divided into three domains: left waveguide, nonlinear unit cells, and right waveguide. The energy in each area is then calculated by summing up the kinetic energy of each mass and the potential energy of each linear and cubic spring.

$$E_{total} = E_L + E_{NL} + E_R \tag{13}$$

$$\eta_{L-R} = \frac{E_R}{E_{total}} \tag{14}$$

$$\eta_{R-L} = \frac{E_L}{E_{total}} \tag{15}$$

Since there is no damping, the total energy remains unchanged. Therefore, the transmission ratio is the transmitted energy, for example the energy in the right waveguide if L-R propagation, divided by the total energy, as shown in equation (14).

In the simulation, we record the energy level in each of the three domains through time. Figure 9(a) and (b) depict one example of the energy transmission pattern for L-R and R-L propagation of a signal with the frequency of 17 rad/s and the amplitude of 0.0002m, which falls in the non-reciprocity range of the associated dispersion curve shown in Figure 5(c). EL, ENL, ER refer to the ratio of the energy in left, nonlinear, and right domain to the total energy respectively.

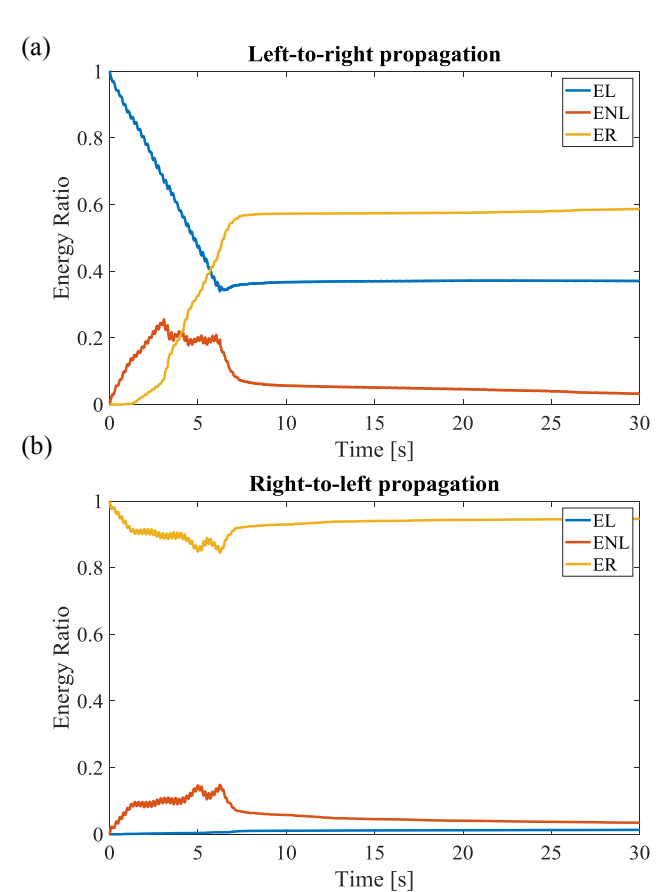
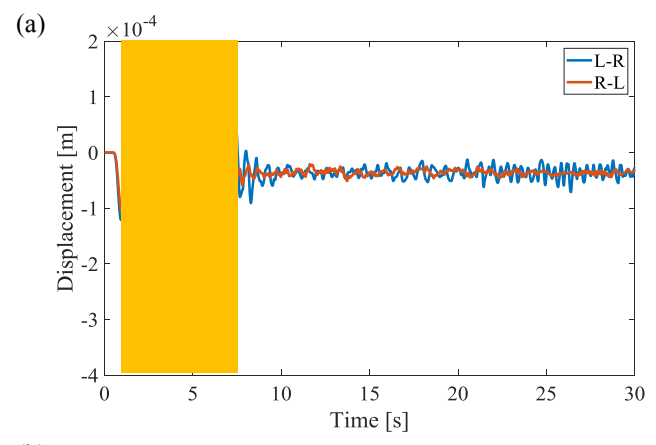


Figure 9. (a) The energy transmission pattern for L-R. Around 60% of the energy passes through the nonlinear unit cells. (b) The energy transmission pattern for R-L. Less than 2% of the energy passes through the nonlinear unit cells.

In Figure 9(a), L-R propagation, the signal is excited in the left waveguide. The wave travels through the nonlinear unit cell domain, and approximately 60% of the energy reaches the right waveguide at the end of the simulation. Less than 5% of energy remains in the nonlinear unit cells. In Figure 9(b), R-L propagation, the signal is excited in the right waveguide. However, less than 2% of energy penetrates the nonlinear unit cells and reaches the other waveguide. Most of the energy is reflected back to the right waveguide.



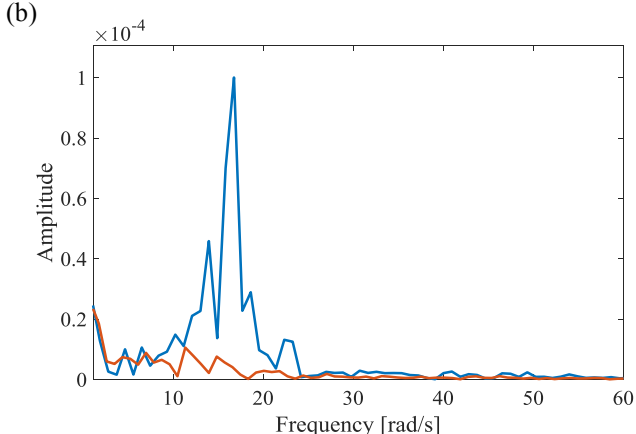


Figure 10. (a) The time response receiving signal. (b) The frequency response of the receiving signal. Obtained by conducting FFT over the highlighted region in Fig. 10(a).

Similarly, we study the time response of the transmitted signal. Figure 10(a) and (b) presents the response of the first mass in the receiver waveguide in displacement and frequency domain. In Figure 10(a), the yellow highlighted area records the transmitted signal. It is clear that there is big difference in the response amplitude between L-R and R-L. Note that, the response after the yellow area is only noises due to the residual energy of the adjacent nonlinear unit cell. In Figure 10(b), the frequency response is obtained by conducting FFT analysis over the highlighted area. The L-R transmitted signal still maintains the sending frequency dominating, while the R-L transmitted signal can be treated as noise.

#### **CONCLUSIONS**

The proposed system broke reciprocity with a passive manner. It contains nonlinearity and geometric asymmetry that rose the dispersion relationship curve to different levels for different directions. Therefore, when the frequency fell in the range between the passband edges of the asymmetrical dispersion curves, the wave is allowed to propagate in one way but not the other, where giant non-reciprocity is observed. The frequency response showed that the signal maintained its source frequency in the chain.

The next steps on this study will be to further optimize the system parameters to break the reciprocity over a larger range of frequency and conduct associated experiment.

#### **ACKNOWLEDGMENTS**

The authors would like to thank the National Science Foundation for support of this research under Emerging Frontiers in Research and Innovation (EFRI) Grant No. 1741565.

#### **REFERENCES**

- [1] Helmholtz, H. v., 1860, "Theorie der Luftschwingungen in Röhren mit offenen Enden," Journal für die reine und angewandte Mathematik, 57, pp. 1-72.
- [2] Strutt, J., 1871, "Some general theorems relating to vibrations," Proceedings of the London Mathematical Society, 1(1), pp. 357-368.
- [3] Casimir, H. B. G., 1945, "On Onsager's principle of microscopic reversibility," Reviews of Modern Physics, **17**(2-3), p. 343.
- [4] Onsager, L., 1931, "Reciprocal relations in irreversible processes. I," Physical review, **37**(4), p. 405.
- [5] Cummer, S. A., Christensen, J., and Alù, A., 2016, "Controlling sound with acoustic metamaterials," Nature Reviews Materials, 1(3), p. 16001.
- [6] Fleury, R., Sounas, D., Haberman, M. R., and Alu, A., 2015, "Nonreciprocal acoustics," Acoustics Today, **11**(EPFL-ARTICLE-223074), pp. 14-21.
- [7] Nassar, H., Xu, X., Norris, A., and Huang, G., 2017, "Modulated phononic crystals: Non-reciprocal wave propagation and Willis materials," Journal of the Mechanics and Physics of Solids, 101, pp. 10-29.
- [8] Trainiti, G., and Ruzzene, M., 2016, "Non-reciprocal elastic wave propagation in spatiotemporal periodic structures," New Journal of Physics, **18**(8), p. 083047.
- [9] Liang, B., Guo, X., Tu, J., Zhang, D., and Cheng, J., 2010, "An acoustic rectifier," Nature materials, 9(12), p. 989.
- [10] Liang, B., Yuan, B., and Cheng, J.-c., 2009, "Acoustic diode: Rectification of acoustic energy flux in one-dimensional systems," Physical review letters, **103**(10), p. 104301.
- [11] Bunyan, J., Moore, K. J., Mojahed, A., Fronk, M. D., Leamy, M., Tawfick, S., and Vakakis, A. F., 2018, "Acoustic nonreciprocity in a lattice incorporating nonlinearity, asymmetry, and internal scale hierarchy: Experimental study," Physical Review E, **97**(5), p. 052211.

- [12] Fronk, M. D., Tawfick, S., Daraio, C., Vakakis, A. F., and Leamy, M. J., "Non-Reciprocity in Structures With Nonlinear Internal Hierarchy and Asymmetry," Proc. ASME 2017 International Design Engineering Technical Conferences and Computers and Information in Engineering Conference, American Society of Mechanical Engineers, pp. V008T012A023-V008T012A023.
- [13] Li, N., and Ren, J., 2014, "Non-reciprocal geometric wave diode by engineering asymmetric shapes of nonlinear materials," Scientific reports, 4, p. 6228.
- [14] Darabi, A., and Leamy, M. J., 2017, "Clearance-type nonlinear energy sinks for enhancing performance in

- electroacoustic wave energy harvesting," Nonlinear Dynamics, 87(4), pp. 2127-2146.
- [15] Hussein, M. I., Leamy, M. J., and Ruzzene, M., 2014, "Dynamics of phononic materials and structures: Historical origins, recent progress, and future outlook," Applied Mechanics Reviews, **66**(4), p. 040802.
- [16] Narisetti, R. K., Leamy, M. J., and Ruzzene, M., 2010, "A perturbation approach for predicting wave propagation in one-dimensional nonlinear periodic structures," Journal of Vibration and Acoustics, **132**(3), p. 031001.